SCIENCE CHINA
Life Sciences

•RESEARCH PAPER•

June 2020 Vol.63 No.6: 875–885
https://doi.org/10.1007/s11427-020-1675-x

An optical brain-to-brain interface supports rapid information transmission for precise locomotion control

Lihui Lu[1,2,3], Ruiyu Wang[3,4,5] & Minmin Luo[2,3,5,6,7*]

[1]*School of Life Sciences, Tsinghua University, Beijing 100084, China;*
[2]*Tsinghua-Peking Center for Life Sciences, Tsinghua University, Beijing 100084, China;*
[3]*National Institute of Biological Sciences (NIBS), Beijing 102206, China;*
[4]*School of Life Sciences, Peking University, Beijing 100871, China;*
[5]*Peking University-Tsinghua University-NIBS Joint Graduate Program, Beijing 102206, China;*
[6]*Chinese Institute for Brain Research, Beijing 102206, China;*
[7]*Tsinghua Institute of Multidisciplinary Biomedical Research (TIMBR), Beijing 102206, China*

Received January 16, 2020; accepted March 5, 2020; published online March 20, 2020

Brain-to-brain interfaces (BtBIs) hold exciting potentials for direct communication between individual brains. However, technical challenges often limit their performance in rapid information transfer. Here, we demonstrate an optical brain-to-brain interface that transmits information regarding locomotor speed from one mouse to another and allows precise, real-time control of locomotion across animals with high information transfer rate. We found that the activity of the genetically identified neuromedin B (NMB) neurons within the nucleus incertus (NI) precisely predicts and critically controls locomotor speed. By optically recording Ca^{2+} signals from the NI of a "Master" mouse and converting them to patterned optogenetic stimulations of the NI of an "Avatar" mouse, the BtBI directed the Avatar mice to closely mimic the locomotion of their Masters with information transfer rate about two orders of magnitude higher than previous BtBIs. These results thus provide proof-of-concept that optical BtBIs can rapidly transmit neural information and control dynamic behaviors across individuals.

brain-to-brain interface, locomotion, nucleus incertus, fiber photometry, optogenetics, support vector machine (SVM) classifier

Citation: Lu, L., Wang, R., and Luo, M. (2020). An optical brain-to-brain interface supports rapid information transmission for precise locomotion control. Sci China Life Sci 63, 875–885. https://doi.org/10.1007/s11427-020-1675-x

INTRODUCTION

Communications between two humans or animals conventionally depend on sensory systems for vision, audition, olfaction, or touch. Emerging new technologies such as brain-to-brain interfaces (BtBIs) have been proposed to revolutionize the method of communicating the subject's intention to another one or others by bypassing direct sensory exchange (Deadwyler et al., 2013; Grau et al., 2014; Lee et al., 2017; Li and Zhang, 2016; Mashat et al., 2017; Pais-Vieira et al., 2013; Rao et al., 2014; Yoo et al., 2013; Zhang et al., 2019b). A BtBI consists of two parts: a decoder that retrieves useful information from the neural activity of the source brain and an encoder that converts the source information to appropriate change in the neuronal activity in the target brain. Nicolelis and colleagues provided initial demonstrations that, by retrieving electrophysiological signals via multi-channel recordings from one brain and then influencing the neuronal activity in another brain via intracortical electrical microstimulation (ICMS), they enabled one animal to bias the performance of another animal by ~10%, which suggests the exciting concept of direct in-

*Corresponding author (email: luominmin@nibs.ac.cn)

formation transfer between brains through BtBIs (Pais-Vieira et al., 2013). They further demonstrated that multiple animal brains can be integrated into a Brainnet that self-adapts to achieve a common behavioral goal for group of animals (Pais-Vieira et al., 2015; Ramakrishnan et al., 2015). Deadwyler et al. showed that neural firing patterns encoding usable memory can be extracted from the hippocampus of a trained rat, and then be inserted into the same regions of another untrained rat via electrical stimulation to enhance the performance in a memory-related task (Deadwyler et al., 2013). Several recent studies implemented BtBIs between two or three human subjects using noninvasive technologies such as electroencephalography (EEG) and transcranial magnetic stimulation (TMS), in which sensory perception or finger move intention could be directly transferred from one brain to another (Jiang et al., 2019; Lee et al., 2017; Mashat et al., 2017; Rao et al., 2014; Stocco et al., 2015; Yoo et al., 2013). In addition to information transfer between two brains of the same species, several groups also demonstrated that movement commands can be extracted from human brains via EEG and transferred to the cockroach antenna nerve or rat brains through electrical stimulation or focused ultrasound (Li and Zhang, 2016; Yoo et al., 2013; Zhang et al., 2019b).

However, BtBIs have thus far required the use of demanding techniques for long-term, multi-channel recordings or EEG to decode the information from the source brain, and have been limited by low rates of information transfer to a target neural circuit (Tehovnik and Teixeira-e-Silva, 2014). Multi-channel single-unit recordings are technically challenging and often lack cell-type specificity. EEG recordings are inaccessible to subcortical areas to precisely decode specific intention (Chaudhary et al., 2016; De Massari et al., 2013). Moreover, EEG recordings of steady-state visually evoked potentials require external visual stimulation to generate the brain activity rather than the internal neural activity (Hong and Khan, 2017). Another challenge lies in the need of feeding the electrophysiological information, once decoded, into correct cell types and neural circuits. Due to these technical limitations, the information transfer rates were often in the low range of 0.004–0.033 bits s^{-1} (Grau et al., 2014; Pais-Vieira et al., 2013; Tehovnik and Teixeira-e-Silva, 2014). Using a BtBI to control locomotion appears to be particularly difficult, since locomotion involves frequent starts, stops, and continuous changes in velocity at a sub-second scale. Demonstrating the possibility of real-time, precise control of locomotor speed will represent a major step toward realizing the full potential of BtBIs.

Here, we set up an optical BtBI that is based on population neuron activity recording with fiber photometry of Ca^{2+} signals and optogenetic stimulation of the same neuron type in the target brain to drive locomotor commands. Specifically, we extracted locomotor speed parameters from the neuromedin B (NMB)-expressing neurons in the nucleus incertus (NI) of the "Master" mouse. We then decoded the optical signals using support vector machine (SVM)-trained model in real time. Finally we transmitted the signals directly to the brain of the "Avatar" mouse via optogenetics. This optical BtBI produced striking synchrony between the locomotor activity of the Master mouse and that of the Avatar mouse with high information transfer rate of over 4 bits s^{-1}, which is 2 to 3 orders of magnitude higher than that transferred by electrophysiology-based BtBI.

RESULTS

Neural basis of the optical BtBI that transfers locomotion speed

We chose to implement an optical BtBI based on our recent findings that NMB-expressing neurons in the NI integratively control locomotion, arousal, and hippocampal theta (Lu et al., 2020). To test how precisely the activity of NI NMB neurons predicts locomotor speed, we expressed the genetically-encoded Ca^{2+} indicator GCaMP6 in NI NMB neurons, and then applied fiber photometry to measure GCaMP fluorescence changes in these neurons and simultaneously monitored locomotor speed (Figure 1A–C). In a head-fixed preparation that allowed the mouse to walk on a wheel treadmill, the fluctuations of GCaMP6 signals closely matched the observed changes in locomotor speed (Figure 1D). The GCaMP6 signals during locomotion are significantly higher than that in rest (Wilcoxon matched-pairs signed rank test, $P<0.01$; Figure 1E). Segmenting and aligning the GCaMP6 signals with the onset and offset of animal locomotion revealed that the rise and decay of GCaMP6 signals were synchronized with the acceleration and deceleration events, with the rise preceding the locomotor initiation by ~0.9 s, and the decay lagging behind the locomotor termination by ~1 s (Figure 1F and G). We did not observe any clear changes in fluorescence when the GFP-expressing mice walked (Figures 1H and I), indicating that the GCaMP6 fluorescence changes reflected Ca^{2+} signals, not artifacts of animal movement. Using the GCaMP6 signals of NI neurons as input, a linear decoder algorithm could predict running speed with high accuracy (Person's correlation coefficient=0.82; Figure 1J). While the polynomial nonlinear regression method performed similarly (Person's correlation coefficient=0.83), a decoder using artificial neural network (ANN) produced significantly higher prediction quality than the linear decoder (Person's correlation coefficient=0.85 for the ANN; non-parametric Dunn's multiple comparisons test, $P<0.01$; Figure 1J and K). Using confusion matrices to visualize the performance of the three decoders on predicting locomotor speed from Ca^{2+} signals, we found that the ANN decoder improved especially when

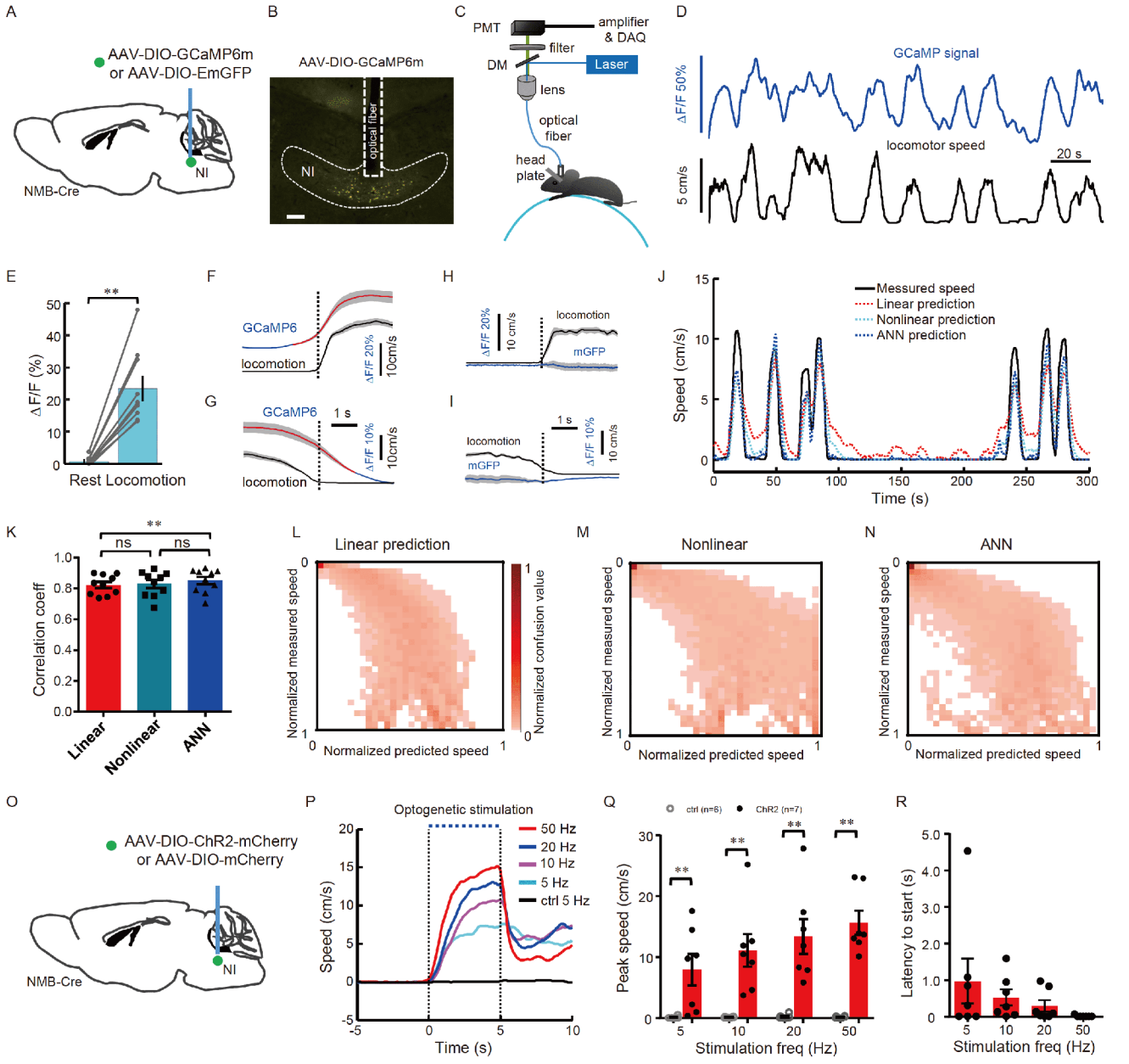

Figure 1 Neural basis of the optical brain-to-brain interface that transfers locomotor speed information. A, Schematic of fiber photometry recording of GCaMP6-expressing nucleus incertus (NI) neuromedin B (NMB) neurons. The blue color bar indicates fiber optic. AAV, adeno-associated virus; DIO, double-floxed inverted open reading frame. B, A representative coronal section showing GCaMP6m expression pattern in the NI and the site of optical fiber placement for recording Ca^{2+} signals. Scale bar, 200 μm. C, A fiber photometry system recorded Ca^{2+} transients from GCaMP6-expressing NI neurons of a NMB-Cre mouse running on a wheel treadmill. DM, dichroic mirror; PMT, photomultiplier tube; DAQ, data acquisition. D, Representative recording traces of GCaMP fluorescence change (upper) and the matched locomotor speed of a head-fixed mouse (lower). The correlation coefficient between GCaMP fluorescence change and animal locomotor speed is 0.81±0.02, mean±SEM (n=10 mice). E, Significantly higher Ca^{2+} signals when a mouse actively moved (Wilcoxon matched-pairs signed rank test; n=10 mice). F and G, Average Ca^{2+} signals (blue) and running speed (black) as a function of time relative to locomotor onset and termination. The rise of Ca^{2+} signals preceded the locomotor onset for about 0.9 s (0.93±0.15 s; mean±SEM) and the decay of Ca^{2+} signals lagged behind the termination of locomotion for about 1 s (1.02±0.13 s; n=10 mice). Red segments indicate statistically significant increase from the baseline (P<0.01; multivariate permutation test). H and I, Population data of the EmGFP-expressing control animals during acceleration (H) and deceleration (I) events (n=13 mice). J, The performance of different decoders on predicting locomotor speed from GCaMP6m signals of NI neurons. Black line, measured speed; dashed red line, linear prediction; dashed cyan line, polynomial nonlinear prediction (abbreviated as "nonlinear"); dashed blue line, artificial neural network (ANN) prediction. K, Correlation coefficient for predicted locomotor speed using linear (red), nonlinear (cyan), or ANN (blue) prediction model (non-parametric Dunn's multiple comparisons test, n=10 mice). L–N, Average speed confusion matrix using normalized measured speed and linear prediction speed (L), nonlinear prediction speed (M), or ANN prediction speed (N). Color bar indicates confusion values that were normalized by row. O, Schematic of optogenetic activation of NI NMB neurons. The blue color bar indicates fiber optic. P, The average locomotor speed of head-fixed mice when they were delivered laser pulses at different stimulation frequency (ctrl, n=6 mice; ChR2, 7 mice). Controls are mCherry-expressing mice. Q, Quantification of maximal speed during activation of NI NMB neurons with different stimulation frequency (Mann Whitney test). R, Quantification of onset latency. **, P<0.01; ns, not significant. Error bars (E, K, Q, R) and shaded areas (F–I) indicate SEM.

the locomotor speed was high (Figure 1L–N).

Next, we investigated the effect of optogenetically activating NI NMB neurons at different frequency on animal locomotor speed. We expressed the light-sensitive cation channel ChannelRhodopsin-2 (ChR2) in NI neurons following the infusion of *AAV-DIO-ChR2-mCherry* vectors into the NI of NMB-Cre mice (Figure 1O). We then implanted an optical fiber to deliver trains of light pulses of various frequencies into the NI of head-fixed behaving mice. Optogenetic stimulation of NI neurons reliably triggered locomotion and enhanced locomotor speed in a frequency-dependent manner (Figure 1P). Stimulation at 5 Hz produced small but statistically significant increases, and those at higher frequencies (10, 20, 50 Hz) led to greater increases in locomotor speed (Mann Whitney test, $P<0.01$; Figure 1Q). The effect was immediate, with a latency of less than 0.5 s at higher frequencies (Figure 1R). Delivering light pulses into the mCherry-expressing control mice did not change mouse locomotion (Figure 1P–R), which confirmed the requirement for ChR2-mediated neuronal activation. Therefore, using an optogenetic approach, we are able to control animal locomotor speed by adjusting the stimulation frequency.

An optical BtBI achieves real-time control of locomotion across individuals

To build an optical BtBI that transfers locomotor speed, we recorded the Ca^{2+} signals from the NI of a GCaMP6-expressing mouse (termed "Master") and optogenetically stimulated the NI neurons of a ChR2-expressing mouse (termed "Avatar") or a mCherry-expressing control mouse (termed "non-responder") (Figure 2A; Figure S1A in Supporting Information). To minimize any potential complications from body turning and to minimize interference between mice, both mice were head-fixed and allowed to walk freely on wheel treadmills situated ~1.5 m apart. Before the start of the experiment, the mouse was subjected to a pretrial in which its Ca^{2+} signals and locomotor speeds were recorded simultaneously for about 20 min to construct a template. We used a SVM to predict the start and the stop of locomotion (the accuracy of SVM predictor is 98.19%) and then transformed the analog Ca^{2+} signals into digital signals as brief light pulses at 20–50 Hz (Figure 2B; Figure S1B in Supporting Information).

We tested 14 Master-Avatar dyads and found that the locomotor activity of the Master mouse and that of the Avatar mouse was strikingly synchronous (Figure 2C; Movie S1 in Supporting Information). By contrast, no such synchrony was observed in the Master-non-Responder control dyads (Figure S2A in Supporting Information). Calculating the cross-correlation between the locomotor speeds of the Master-Avatar dyads revealed a maximum correlation efficient of over 0.9, and a mean value of ~0.68 (n=14 dyads), which is significantly higher than the near random value of control dyads (0.03; n=12 dyads; Mann Whitney test, $P<0.0001$; Figure 2D and E; Figure S2B in Supporting Information). We observed a prominent diagonal distribution in the confusion matrix containing information about Master and Avatar locomotor speed, which indicates strong overall synchrony (Figure 2F; Figure S2C in Supporting Information). We calculated the area under the receiver operating characteristics (AUROC) curve to quantify the accuracy of behavioral control (Fawcett, 2006). By defining stationary as 0 and movement as 1, we revealed that the AUROC of the Master-Avatar dyads is 0.77, which is significantly higher than the near-random value (0.46) of the control dyads (Figure 2G and H, Mann Whitney test, $P<0.0001$). Although a mCherry-expressing mouse ("non-responder") produced occasional locomotor responses when a Master mouse was also walking, the true positive rate of the Master-Avatar dyads (79%) is significantly higher than that of the control dyads (18%, Mann Whitney test, $P<0.0001$) (Figure 2I; Figure S2D in Supporting Information).

Aligning the Avatar's locomotor speed to the acceleration and deceleration events of the Master revealed only a small delay (0.45 s for onset and 1.30 s for offset; Figure 3A–E). To quantify the rate of effective information transmission from a Master mouse to an Avatar mouse, we calculated the information transfer rate of the optical BtBI using Bit rate (bits per second; bps) based on the mutual information—a standard in information theory (Figure S3 in Supporting Information) (Hangya et al., 2009; Jiang et al., 2019; Schlogl et al., 2003; Shannon, 1948; Tehovnik et al., 2013). When the Master moved and triggered the movement of the Avatar mouse, the information transfer rate rapidly increased, reaching over 4 bps during sustained walking (Figure 3F–I). The mean information transfer rate of the Master-Avatar dyads is 4.1 bps, which is significantly higher than that of the control dyads (0.1 bps, Mann Whitney test, $P<0.0001$; Figure 3J; Figures S2E–L and S3 in Supporting Information).

DISCUSSION

The present study, to the best of our knowledge, provides the first demonstration that an optical BtBI can transfer information regarding locomotor speed across the NI of two mice to achieve real-time control of locomotion. We note that the information rate (4.1 bps) of the BtBI here is at least 2 orders of magnitude (200–1000×) higher than the estimated information rates reported for multi-channel recording-based BtBIs (Pais-Vieira et al., 2013; Tehovnik and Teixeira-e-Silva, 2014). It is also higher than the information transfer rate of EEG-based brain-computer interface (BCI) used to control cursor movement or robot hand, or to select letters, which commonly fell below 1 bps (Baek et al., 2019; Chen et

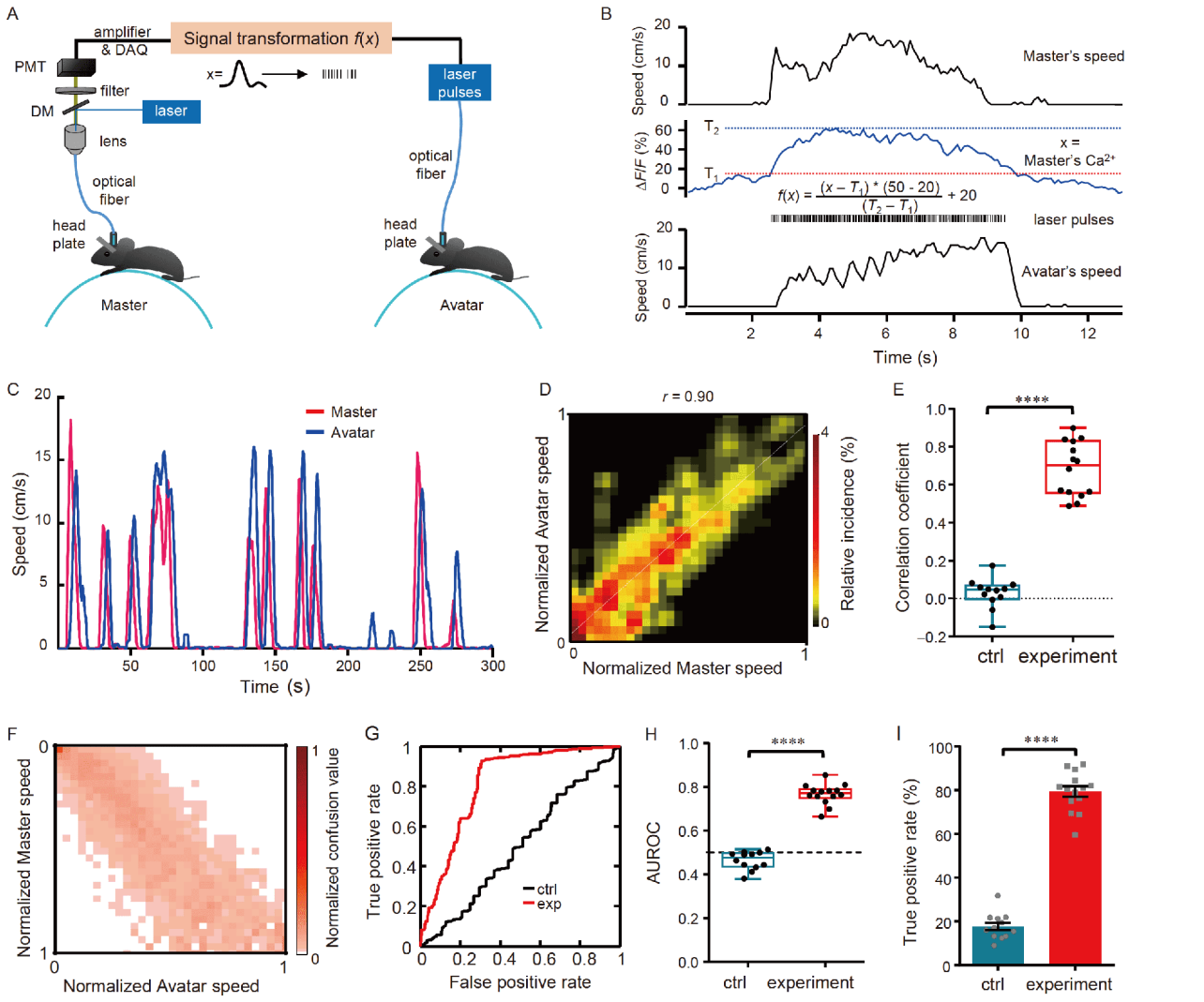

Figure 2 An optical BtBI transmits information regarding locomotor speed across brains. A, Schematic of the optical BtBI. We used fiber photometry to record the population Ca^{2+} signals of NI neurons from the Master mouse, transformed the signals to blue laser pulses, and delivered the laser pulses into the NI of the Avatar mouse. DM, dichroic mirror; PMT, photomultiplier tube; DAQ, data acquisition. B, Example traces showing, from the top to the bottom, the locomotor speed of the Master, the Ca^{2+} signal of NI neurons from the Master, the signal transformation formula, frequency modulation of light pulses, and the locomotor speed of the Avatar. C, Locomotor speeds of a representative BtBI dyad. D, Correlation between Master's speed and Avatar's speed (a representative BtTI dyad). Relative incidence means the probability of specific Master's speed and the corresponding Avatar's speed on all recording data. E, Group data showing the Pearson correlation coefficients of the control group (n=12 dyads) and the BtBI group (n=14 dyads). The control group consisted of GCaMP6-expressing Masters and mCherry-expressing non-responder mice. F, Average speed confusion matrix that consists of normalized Master speed and Avatar speed for every time point across all BtBI dyads (n=14). Color bar indicates confusion values normalized by row. G, Receiver Operating Characteristics (ROC) curves for a control dyad and an experiment dyad. The ROC curve is based on binarized data, with 0 indicating stationary and 1 movement. H, Group data showing the area under the ROC (AUROC) of the control group and the BtBI group. I, Group data showing the true positive rate of the control group and the BtBI group. Error bars (E, H, I) indicate SEM. ****, P<0.0001; Mann Whitney test.

al., 2019; Han et al., 2019; Jin et al., 2011; Khalaf et al., 2019; LaFleur et al., 2013; Meng et al., 2018; Tehovnik and Chen, 2015; Tehovnik et al., 2013; Zhang et al., 2019a). Fast information rate is essential, because locomotor speeds often change with subsecond resolution. BtBIs with low information rates (<0.02 bps) can bias behaviors over seconds but cannot precisely control rapidly changing behaviors such as locomotion.

Our results emphasize the importance of choosing appropriate neural circuits and of choosing suitable circuit-probing technologies when building a high-performance BtBI. First, the choice of brain structures is important for implementing task-relevant BtBIs. Here we collected neuronal signals that precisely report locomotor state and control locomotor speed from the genetically-identified NMB neurons in the NI of the pons. Second, our choice of fiber photometry of Ca^{2+} signals offers several advantages: (1) it stably records the population neuronal activity of specific cell-type that performs similar functions; (2) it has high signal-to-noise ratio (SNR); (3) it is easy to implement, since it bypasses the challenging task of

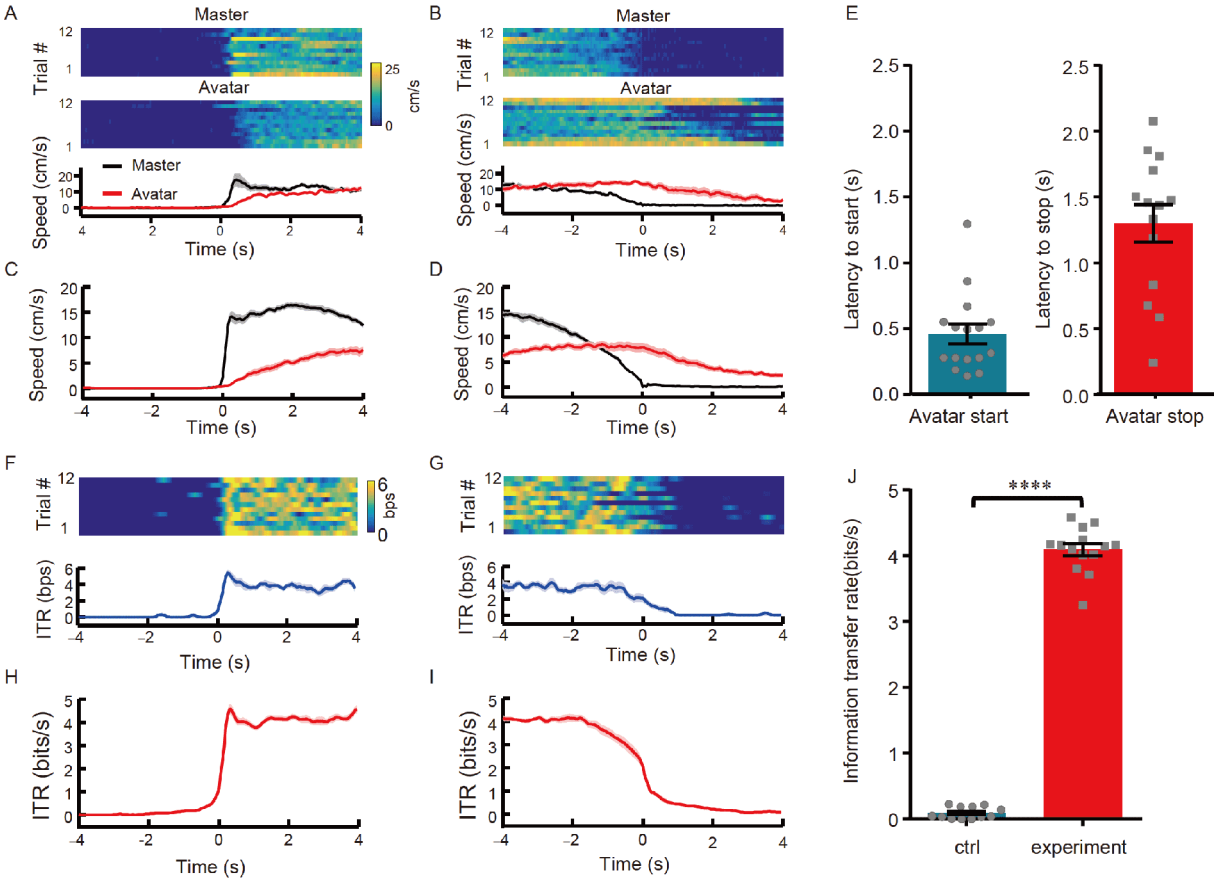

Figure 3 Evaluation of information transfer rate of the optical BtBI. A and B, Avatar followed Master during the acceleration (A) or deceleration (B) events of the Master mouse. Heatmaps illustrate the locomotor activity of the dyad for 12 events. Plots show the average speed of the two animals as a function of time relative to the event onset. C and D, Average locomotor speed of the total test group (n=14 dyads) during acceleration (C) and deceleration (D). E, Quantification of latency to start and latency to stop of Avatars. F and G, Information transfer (IT) rates (bits s^{-1}, bps) from the Master to the Avatar. We measured the rate of mutual information between the locomotor motor speed of the Master and that of the Avatar during the acceleration (F) and deceleration (G) events. Heatmaps in the top panel show the information transfer rate of individual trials for one representative dyad. Bottom panels show the average information rates for the dyad as a function of time relative to the event onset and offset. H and I, Average information rate of the total test group (n=14 dyads). J, Quantification of information transfer rate of the control group (n=12 dyads) and the BtBI group (n=14 dyads). Mean information transfer rate is calculated during 0.5–3.5 s with data showed in H and Figure S2K in Supporting Information. Shaded areas (A–D, F–I) and error bars (E, J) indicate SEM. ****, P<0.0001; Mann Whitney test.

multi-channel single-unit recording from behaving animals and obviates the need for the extensive decoding of information from large datasets (Hong and Khan, 2017). Indeed, we achieved high decoding accuracy (98%) using the simple method of SVM training of Ca^{2+} signals and locomotor speed. Finally, we used optogenetic stimulation, which also enjoys the advantage of fine-tuning the activity of a genetically defined set of neurons in a given brain area (Boyden et al., 2005; Roseberry et al., 2016).

The optical BtBI can be improved in several aspects. Increasing the number of sensors and command channels using multi-channel fiber photometry and multi-channel optogenetics would likely further enhance the accuracy (Guo et al., 2015; Hong and Khan, 2017). In addition to the simple linear transfer function, nonlinear transformation functions and ANNs may improve the performance of BtBt by optimizing the conversion of physiological signals to frequency modulation signals for photostimulation. In addition to optogenetic activation, co-expressing optogenetic probes for activation and inhibition might allow more precise control using different light wavelengths. Further discoveries about the roles of other brain centers in controlling additional aspects of locomotion, such as body turning and backward movement, should facilitate the development of BtBIs that allow one to fully control the locomotion of other individuals, within or even across species.

Our results have several implications in multiple basic and clinical research domains. By extracting information from genetically-identified neural activity from relevant brain areas, optical BtBI and brain-computer interface (BCI) may enable rapid information transfer of other behaviorally relevant signals, such as sensory perception, motor control, emotion, and even memory, and thus be used for the control of peripheral neuroprosthetic devices and the sharing cog-

nitive load to improve human performance (Maksimenko et al., 2018). Much more broadly, this demonstration of fast information sharing between brains invites discussion about the concept of neural privacy and other potential ethical issues, and even about philosophical concerns relating to free will and individualism (Hildt, 2015, 2019; Kyriazis, 2015; Trimper et al., 2014).

MATERIALS AND METHODS

Animals

All procedures were conducted with the approval of the Animal Care and Use Committee of the National Institute of Biological Sciences, Beijing in accordance with governmental regulations of China. All mice were maintained on a 12 h reverse light/dark cycle (light on 8 p.m.) and given *ad libitum* access to chow and water. NMB-Cre mice (Lu et al., 2020) were maintained on a mixed FVB/C57Bl/6J background. Either sex of mice was used in this study. All procedures were conducted during the dark cycle.

Virus production and injection

The *pAAV-EF1a-DIO-hChR2(H134R)-mCherry* (simplified as *AAV-DIO-ChR2-mCherry*) construct was a gift of K. Deisseroth (Stanford University; Addgene plasmid 20297). In the *AAV-DIO-mCherry* construct, the ChR2 sequence was removed from the *AAV-DIO-ChR2-mCherry* construct. We constructed the plasmid *pAAV-EF1a-DIO-GCaMP6m*, *pAAV-EF1a-DIO-EmGFP* by replacing the coding region of *ChR2-mCherry* in the *pAAV-EF1a-DIO-hChR2(H134R)-mCherry* plasmid with that of *GCaMP6m* (a gift from Douglas Kim; Addgene Plasmid #40754) and that of enhanced membrane green fluorescent protein (*EmGFP*; a gift from Connie Cepko; Addgene Plasmid #14757). AAV vectors were packaged into serotype 2/9 vectors, which consisted of AAV2 ITR genomes pseudotyped with AAV9 serotype capsid proteins. AAV vectors were replicated in HEK293 cells with the triple plasmid transfection system and purified by cesium chloride-density gradient centrifugation and then desalination via dialysis against a physiological buffer, resulting in AAV vector titers of about 2×10^{12} particles mL^{-1}.

We injected the virus and implanted optical fiber following a previously described procedure (Lu et al., 2020). Briefly, we performed stereotaxic injections using standard stereotaxic instruments (RWD, Shenzhen, China) under Avertin anesthesia (i.p. 250 mg kg^{-1}). We made a small craniotomy and then lowered a glass pipette which filled with AAV to the NI (coordinates 5.4 mm from Lambda, 0 mm from the midline, and 3.6 mm ventral to Lambda). We infused 150–300 nL virus solution (speed at 46 nL min^{-1}) using a microsyringe pump (Nanoliter 2000 Injector with the Micro4 controller, WPI, USA) and left the injection pipette in place for five additional minutes before withdrawing it slowly. We then implanted an optical fiber with custom-built fiber connector (fiber: 0.39 numerical aperture, 200 μm diameter; Thorlabs, USA) into the NI, and fixed the optical fiber and a custom-made titanium head-plate to the skull with cyanoacrylate adhesive (TONSAN 1454, Beijing, China) and dental cement. Mice were allowed to recovery and virus expression for 2 weeks.

Fiber photometry recording

To record neural activity when the animal was running, we used the fiber photometry recording system set up by ThinkTech, Nanjing, China (Li et al., 2016). Briefly, to record fluorescence signals, laser beam from a 488 nm laser (OBIS 488LS; Coherent, USA) was reflected by a dichroic mirror (MD498; Thorlabs, USA), focused by a 10× objective lens (NA 0.3; Olympus, Japan) and then coupled to an optical commutator (Doric Lenses, Canada). An optical fiber (200 μm diameter, 0.39 NA) guided the light between the commutator and the implanted optical fiber. To minimize bleaching, the laser power was adjusted at the tip of optical fiber to the low level of 10–20 μW. The GCaMP fluorescence was bandpass filtered (MF525-39, Thorlabs) and collected by a photomultiplier tube (R3896, Hamamatsu, Japan). An amplifier (C7319, Hamamatsu) was used to convert the current output from the photomultiplier tube to voltage signals, which was further filtered through a low-pass filter (40 Hz cut-off; Brownlee 440, USA). The fluorescence signals were digitalized at 500 Hz and recorded by a Power 1401 digitizer and Spike2 software (CED, UK). To record from a head-fixed mouse, we allow the mouse to habituate on a wheel treadmill in 1–2 daily sessions (about 30 min per session) prior to recordings. We used a rotary encoder to monitor the movement of the running wheel. The TTL signals from the rotary wheel were collected at 500 Hz (Power 1401, CED, UK).

Optogenetic stimulation

To examine the effects of optogenetic activation of NI neurons, head-fixed mice were habituated on the wheel treadmill for 1–2 daily sessions (about 30 min per session) prior to light delivery. A rotary encoder monitored the movement of the running wheel. For optogenetic stimulation, trains of blue light pulses (473 nm wavelength; 5 ms per pulse at the frequencies of 5/10/20/50 Hz for 5 s; 10–20 mW power measured with continuous light) were delivered through an optical fiber to the NI of ChR2-expressing or mCherry-expressing mice while they were stationary (20–40 s between trials, 20 trials).

Brain-to-brain interface (BtBI)

For fiber photometry recording or optogenetic stimulation, an optical fiber (0.39 numerical aperture, 200 μm diameter; Thorlabs, USA) was placed in a ceramic ferrule and inserted towards the NI of a GCaMP6m-expressing mouse ("Master"), ChR2-expressing mouse ("Avatar"), or a mCherry-expressing control mouse ("non-responder"). Head-fixed mice were allowed to habituate on the wheel treadmill for 1–2 days prior to the experiment. We recorded Ca^{2+} signals from the Master mouse using fiber photometry. Before the start of the experiment, the mouse was subjected to a pre-trial in which its Ca^{2+} signals and movement speeds were recorded simultaneously for approximately 20 min. We binned data at 10 Hz and classified the movement state of the animal into four modes: halt, acceleration, running, and deceleration. We then used Ca^{2+} signals and speed mode data to train a SVM that predicts the mode which would be used to determine the timing of optical stimulation during the experimentation. We extracted four features of Ca^{2+} signal during a 1.5 s time window (i.e., every 0.1 s, the most recent 1.5 s segment from Ca^{2+} signal was analyzed to predict the timing of stimulation): (1) maximum slope defined as the maximum of the diff of Ca^{2+} signal, (2) rise rate defined as the last Ca^{2+} signal value minus the first Ca^{2+} signal values, (3) up rate defined as peak minus nadir and then divided by the duration between them, and (4) integral defined as the sum of Ca^{2+} signal values. The size of the feature vector was 19 points (15 points of Ca^{2+} signal and four features extracted from Ca^{2+} signal during a 1.5 s time window). We trained two models with the MATLAB *fitcsvm* function: the first model was trained by halt and acceleration movement mode data and the corresponding Ca^{2+} signal features data; the second model was trained by running and deceleration movement mode and the corresponding Ca^{2+} signal features. We also calculated the Ca^{2+} signal value (T_1) at the first acceleration mode following halt state and the maximum Ca^{2+} signal (T_2). We used the models for instantaneous and continuous prediction of movement mode with the Ca^{2+} signal acquired in real time. Using two Arduinos (Uno R3, Shenzhen, China) and a customized MATLAB program (sampling rate is 10 Hz, sliding window is 1.5 s, Figure S1B in Supporting Information), we transformed the analog signal into TTL pulses with either 0 Hz or 20–50 Hz, according to the input-output relationship defined by the following formula: $f(x)=\frac{(x-T_1)+(50-20)}{T_2-T_1}+20$, in which x indicates the instantaneous Ca^{2+} signals, T_1 denotes the Ca^{2+} signal value that predicts acceleration, T_2 denotes the maximum value of Ca^{2+} signals. When the SVM predictor predicted acceleration, Arduino 1 transferred an analog voltage signal to Arduino 2, which then transformed the analog^{+} signal into TTL pulses according to the input-output relationship. When the SVM predictor predicted deceleration and the Ca^{2+} signal values were lower than T_1, Arduino 2 terminated TTL signals. The TTL signals triggered laser pulses (5 ms, 10–20 mW) through an optical fiber into the NI of the Avatar mouse or its control non-responder. Individual mice were allowed to walk on a distant running wheel under dim-light with their heads facing same direction. A Power 1401 digitizer and Spike2 software simultaneously recorded the locomotor speed and Ca^{2+} signals from the Master, the TTL signals for laser pulses, and the locomotor speed of the Avatar or its control.

Histology

Mice were killed with an overdose of pentobarbital and perfused intracardially with 0.1 mol L^{-1} phosphate buffer saline and then 4% paraformaldehyde. After cryoprotection in 30% sucrose, coronal sections (50 μm thickness) were cut on a cryostat (Leica CM1950, Germany). The sections were cover-slipped with 50% glycerol and DAPI (1 μg mL^{-1}) in the mounting medium. Fluorescent signals and fiber tracks were imaged with an automated slide scanner (VS120 Virtual Slide, Olympus, Japan).

Quantification and statistical analysis

Analysis of GCaMP6 signals and behavior data were performed using custom functions written in MATLAB (Version 2014a, MathWorks, USA). Statistical tests were carried out using GraphPad Prism software. All data are presented as mean±SEM. For comparisons with only two groups, P values were calculated using Wilcoxon matched-pairs signed rank test, Mann Whitney test, two-sided. *P<0.05; **P<0.01; ***P<0.001; ****P<0.0001; ns, not significant (P>0.05) for all statistical analyses presented in figures.

Analysis of Ca^{2+} signal and locomotor speed

We exported photometry data from Spike2 to MATLAB Mat files for further analysis. We first smoothed the data with the MATLAB *smooth* function and segmented the data based on behavioral events of locomotion initiation or termination. The values of fluorescence change ($\Delta F/F$) were defined as $(F-F_0)/F_0$, where F_0 is the baseline fluorescence signal (1–3 s before locomotion onset or 1–3 s after locomotion offset, Figure 1F–I; average fluorescence during stationary, Figure 1D and J). The transitions between rest and walking were defined as the change between a rest period (< 0.1 cm s^{-1} for at least 2.5 s) and an active period (>1 cm s^{-1} for 3 s and peak speed >7 cm s^{-1}). We used the locomotion initiation and termination time point to trigger the averages of fluorescence signals or the locomotor speeds of Avatar. The Pearson correlation coefficients were computed using the MATLAB *corrcoef* function.

Prediction

The locomotor speed and Ca^{2+} signal (the total recording duration per session was approximately 2 h) were resampled at 10 Hz, Ca^{2+} signal change was calculated according to $(F-F_0)/F_0$, in which F_0 is the average Ca^{2+}signal during stationary. To predict running speed with linear and nonlinear fit, we divided each recoding into two parts, which gave rise to speed vectors V_1 (20 min data) and V_2 (the remainder data) and Ca^{2+} signals F_1 and F_2 with one column, respectively. A linear decoder was implemented as $V_1=p_1\times F_1+p_2$, where p_1 is the coefficient for Ca^{2+} signal value and p_2 is the intercept in the regression. The decoder was then applied to the second fluorescence signals F_2, predicting the corresponding running speed: $V_{predicted}=p_1\times F_2+p_2$. The nonlinear prediction is based on the MATLAB function *polyfit* (the degree is 3), using the same data structure as described for the linear model. To predict with an artificial neural network (ANN), we used the data structure similar to that of linear prediction, except that Ca^{2+} signals F_1 and F_2 are matrix in which each row contains 1.5 s Ca^{2+} signal values. The MATLAB function *fitnet* and *train* were used to build the ANN model using one hidden layer with 10 units, and to train the network with the Levenberg-Marquardt algorithm. The quality of the prediction was established as the Pearson correlation of the real velocity V_2 and the predicted velocity $V_{predicted}$. A confusion matrix contains information about true and predicted locomotor speed done by the MATLAB function *confusionmat* (Figure 1J–N).

Quantification of locomotor speed

For quantifying the effect of optogenetic stimulation on the change in locomotor speed, we calculated the maximal speed during light delivery. Latency was defined as time between stimulus onset and time of speed at 0.1 cm s^{-1}.

Correlation of Master's speed and Avatar's speed

To calculate the correlation of Master's locomotor speed and Avatar's speed, we shifted Avatar's speed according to the time lag which was computed using the MATLAB *xcorr* function, and then normalized to their maximal speed respectively. We calculated the probability of specific Master's speed and the corresponding Avatar's speed on all recording data. The Pearson correlation coefficients between Master's speed and Avatar's speed were computed using the MATLAB *corrcoef* function. A confusion matrix contains information about Master's speed and Avatar's speed done by the MATLAB function *confusionmat.*

ROC of Master's speed and Avatar's speed

To calculate the receiver operating characteristic (ROC), we binned speed data at 20 Hz and then set data as the binary form, 0 indicates stationary and 1 indicates movement. Because the time delay has an effect on estimating the performance of BCI (Billinger et al., 2013; Yuan et al., 2013), we shifted Avatar's speed according to the time lag which was based on the cross-correlation between Master's speed and Avatar's speed. True positive (TP) indicates movement detected in both Master's speed and Avatar's speed; false positive (FP) indicates movement detected only in Avatar's speed but not Master's speed; true negative (TN) indicates stationary states detected in both Master's speed and Avatar's speed; false negative (FN) indicates stationary state detected only in Avatar's speed but not Master's speed. True positive rate (TPR) is defined as $TPR=TP/(TP+FN)\times100$; false positive rate (FPR) is defined as $FPR=FP/(FP+TN)\times100$. To plot ROC curve, we calculated the cumulative TPR and FPR. Accuracy was measured by calculating the area under the ROC curve (AUROC).

Information transfer rate (ITR)

To calculate the information transfer rate of the optical BtBI, we first binned speed data at 20 Hz and then detected initiation and termination of locomotor speed. Latency to start of Avatar was defined as the duration between Master's onset and the first detectable movement of Avatar; latency to stop was defined as the time between Master's offset and the first detectable stationary of Avatar. Because the time delay has an effect on estimating the information transfer rate (Billinger et al., 2013; Yuan et al., 2013), we shifted Avatar's speed according to the time lag which was based on the cross-correlation of Master's speed and Avatar's speed. Using the toolbox of information theory written in MATLAB (Matlabcentral/fileexchange/35625-information-theory-toolbox), we then quantified the amount of information transfer within a sliding 0.25 s time window by calculating the mutual information (Hangya et al., 2009; Schlogl et al., 2003; Shannon, 1948). The mutual information (MI) was defined by the formula $MI=H(X)+H(Y)-H(X, Y)$, where $H(X)$ is the entropy within Master's speed signals, $H(Y)$ is the entropy of the speed of Avatar, $H(X, Y)$ is their joint entropy. The entropy was calculated as $H=-\sum_i p_i \log_2(p_i)$ where p_i denotes the probability of occurrence of the i-th possible value of the locomotor speed for $H(X)$ and $H(Y)$ and the joint probability of certain x and y for $H(X, Y)$. We then determined the information transfer rate by dividing the mutual information with the duration of sliding window (Figure S3 in Supporting Information). We calculated the mutual information with different sliding window, and found that it needs at least 5 points (i.e., 0.25 s), where the maximum mutual information is 2.3219 bit (i.e., both Master's speed and Avatar's speed are different at each time point, Figure S3E in Supporting Information). Therefore, we used 0.25 s as the sliding time window to calculate the ITR.

Compliance and ethics *The author(s) declare that they have no conflict*

of interest. All procedures were conducted with the approval of the Animal Care and Use Committee of the National Institute of Biological Sciences, Beijing in accordance with governmental regulations of China, and conformed with the Helsinki Declaration of 1975 (as revised in 2008) concerning Animal Rights, and followed out policy concerning Informed Consent as shown on Springer.com.

Acknowledgements *We thank J. Snyder for comments and language polish. M.L. is supported by Ministry of Science and Technology of China (2015BAI08B02), the National Natural Science Foundation of China (91432114 and 91632302), and the Beijing Municipal Government.*

References

Baek, H.J., Chang, M.H., Heo, J., and Park, K.S. (2019). Enhancing the usability of brain-computer interface systems. Comput Intel Neurosci 2019, 1–12.

Billinger, M., Daly, I., Kaiser, V., Jin, J., Allison, B.Z., Müller-Putz, G.R., Brunner, C., Allison, B.Z., Dunne, S., Leeb, R., et al. (2013). Is It Significant? Guidelines for Reporting BCI Performance. Towards Practical Brain-Computer Interfaces: Bridging the Gap from Research to Real-World Applications. (Berlin: Springer), pp. 333–354.

Boyden, E.S., Zhang, F., Bamberg, E., Nagel, G., and Deisseroth, K. (2005). Millisecond-timescale, genetically targeted optical control of neural activity. Nat Neurosci 8, 1263–1268.

Chaudhary, U., Birbaumer, N., and Ramos-Murguialday, A. (2016). Brain–computer interfaces for communication and rehabilitation. Nat Rev Neurol 12, 513–525.

Chen, X., Zhao, B., Wang, Y., and Gao, X. (2019). Combination of high-frequency SSVEP-based BCI and computer vision for controlling a robotic arm. J Neural Eng 16, 026012.

De Massari, D., Ruf, C.A., Furdea, A., Matuz, T., van der Heiden, L., Halder, S., Silvoni, S., and Birbaumer, N. (2013). Brain communication in the locked-in state. Brain 136, 1989–2000.

Deadwyler, S.A., Berger, T.W., Sweatt, A.J., Song, D., Chan, R.H.M., Opris, I., Gerhardt, G.A., Marmarelis, V.Z., and Hampson, R.E. (2013). Donor/recipient enhancement of memory in rat hippocampus. Front Syst Neurosci 7, 120.

Fawcett, T. (2006). An introduction to ROC analysis. Patt Recogn Lett 27, 861–874.

Grau, C., Ginhoux, R., Riera, A., Nguyen, T.L., Chauvat, H., Berg, M., Amengual, J.L., Pascual-Leone, A., and Ruffini, G. (2014). Conscious brain-to-brain communication in humans using non-invasive technologies. PLoS ONE 8, e105225.

Guo, Q., Zhou, J., Feng, Q., Lin, R., Gong, H., Luo, Q., Zeng, S., Luo, M., and Fu, L. (2015). Multi-channel fiber photometry for population neuronal activity recording. Biomed Opt Express 6, 3919–3931.

Han, X., Lin, K., Gao, S., and Gao, X. (2019). A novel system of SSVEP-based human–robot coordination. J Neural Eng 16, 016006.

Hangya, B., Borhegyi, Z., Szilagyi, N., Freund, T.F., and Varga, V. (2009). GABAergic neurons of the medial septum lead the hippocampal network during theta activity. J Neurosci 29, 8094–8102.

Hildt, E. (2015). What will this do to me and my brain? Ethical issues in brain-to-brain interfacing. Front Syst Neurosci 9, 17.

Hildt, E. (2019). Multi-person brain-to-brain interfaces: ethical issues. Front Neurosci 13, 1177.

Hong, K.S., and Khan, M.J. (2017). Hybrid brain–computer interface techniques for improved classification accuracy and increased number of commands: a review. Front Neurorobot 11, 35.

Jiang, L., Stocco, A., Losey, D.M., Abernethy, J.A., Prat, C.S., and Rao, R.P.N. (2019). BrainNet: a multi-person brain-to-brain interface for direct collaboration between brains. Sci Rep 9, 6115.

Jin, J., Allison, B.Z., Sellers, E.W., Brunner, C., Horki, P., Wang, X., and Neuper, C. (2011). Optimized stimulus presentation patterns for an event-related potential EEG-based brain–computer interface. Med Biol Eng Comput 49, 181–191.

Khalaf, A., Sejdic, E., and Akcakaya, M. (2019). Common spatial pattern and wavelet decomposition for motor imagery EEG- fTCD brain-computer interface. J NeuroSci Methods 320, 98–106.

Kyriazis, M. (2015). Systems neuroscience in focus: from the human brain to the global brain? Front Syst Neurosci 9, 7.

LaFleur, K., Cassady, K., Doud, A., Shades, K., Rogin, E., and He, B. (2013). Quadcopter control in three-dimensional space using a noninvasive motor imagery-based brain–computer interface. J Neural Eng 10, 046003.

Lee, W., Kim, S., Kim, B., Lee, C., Chung, Y.A., Kim, L., and Yoo, S.S. (2017). Non-invasive transmission of sensorimotor information in humans using an EEG/focused ultrasound brain-to-brain interface. PLoS ONE 12, e0178476.

Li, G., and Zhang, D. (2016). Brain-computer interface controlled cyborg: establishing a functional information transfer pathway from human brain to cockroach brain. PLoS ONE 11, e0150667.

Li, Y., Zhong, W., Wang, D., Feng, Q., Liu, Z., Zhou, J., Jia, C., Hu, F., Zeng, J., Guo, Q., et al. (2016). Serotonin neurons in the dorsal raphe nucleus encode reward signals. Nat Commun 7, 10503.

Lu, L., Ren, Y., Yu, T., Liu, Z., Wang, S., Tan, L., Zeng, J., Feng, Q., Lin, R., Liu, Y., et al. (2020). Control of locomotor speed, arousal, and hippocampal theta rhythms by the nucleus incertus. Nat Commun 11, 262.

Maksimenko, V.A., Hramov, A.E., Frolov, N.S., Lüttjohann, A., Nedaivozov, V.O., Grubov, V.V., Runnova, A.E., Makarov, V.V., Kurths, J., and Pisarchik, A.N. (2018). Increasing human performance by sharing cognitive load using brain-to-brain interface. Front Neurosci 12, 949.

Mashat, M.E.M., Li, G., and Zhang, D. (2017). Human-to-human closed-loop control based on brain-to-brain interface and muscle-to-muscle interface. Sci Rep 7, 11001.

Meng, J., Streitz, T., Gulachek, N., Suma, D., and He, B. (2018). Three-dimensional brain–computer interface control through simultaneous overt spatial attentional and motor imagery tasks. IEEE Trans Biomed Eng 65, 2417–2427.

Pais-Vieira, M., Chiuffa, G., Lebedev, M., Yadav, A., and Nicolelis, M.A.L. (2015). Building an organic computing device with multiple interconnected brains. Sci Rep 5, 11869.

Pais-Vieira, M., Lebedev, M., Kunicki, C., Wang, J., and Nicolelis, M.A.L. (2013). A brain-to-brain interface for real-time sharing of sensorimotor information. Sci Rep 3, 1319.

Ramakrishnan, A., Ifft, P.J., Pais-Vieira, M., Byun, Y.W., Zhuang, K.Z., Lebedev, M.A., and Nicolelis, M.A.L. (2015). Computing arm movements with a monkey brainet. Sci Rep 5, 10767.

Rao, R.P.N., Stocco, A., Bryan, M., Sarma, D., Youngquist, T.M., Wu, J., and Prat, C.S. (2014). A direct brain-to-brain interface in humans. PLoS ONE 9, e111332.

Roseberry, T.K., Lee, A.M., Lalive, A.L., Wilbrecht, L., Bonci, A., and Kreitzer, A.C. (2016). Cell-type-specific control of brainstem locomotor circuits by basal ganglia. Cell 164, 526–537.

Schlogl, A., Keinrath, C., Scherer, R., and Pfurtscheller. (2003). Information transfer of an EEG-based brain computer interface. Proceedings of the 1st International IEEE EMBS, 641–644.

Shannon, C.E. (1948). A mathematical theory of communication. Bell Syst Tech J 27, 623–656.

Stocco, A., Prat, C.S., Losey, D.M., Cronin, J.A., Wu, J., Abernethy, J.A., and Rao, R.P.N. (2015). Playing 20 questions with the mind: collaborative problem solving by humans using a brain-to-brain interface. PLoS ONE 10, e0137303.

Tehovnik, E.J., and Chen, L.L. (2015). Brain control and information transfer. Exp Brain Res 233, 3335–3347.

Tehovnik, E.J., and Teixeira-e-Silva, Z. (2014). Brain-to-brain interface for real-time sharing of sensorimotor information: A commentary. OA Neurosci 2, 1–3.

Tehovnik, E.J., Woods, L.C., and Slocum, W.M. (2013). Transfer of information by BMI. Neuroscience 255, 134–146.

Trimper, J.B., Wolpe, P.R., and Rommelfanger, K.S. (2014). When "I" becomes "We": ethical implications of emerging brain-to-brain

interfacing technologies. Front Neuroeng 7, 1–4.
Yoo, S.S., Kim, H., Filandrianos, E., Taghados, S.J., and Park, S. (2013). Non-invasive brain-to-brain interface (BBI): establishing functional links between two brains. PLoS ONE 8, e60410.
Yuan, P., Gao, X., Allison, B., Wang, Y., Bin, G., and Gao, S. (2013). A study of the existing problems of estimating the information transfer rate in online brain–computer interfaces. J Neural Eng 10, 026014.
Zhang, J., Wang, B., Zhang, C., Xiao, Y., and Wang, M.Y. (2019a). An EEG/EMG/EOG-based multimodal human-machine interface to real-time control of a soft robot hand. Front Neurorobot 13, 7.
Zhang, S., Yuan, S., Huang, L., Zheng, X., Wu, Z., Xu, K., and Pan, G. (2019b). Human mind control of rat cyborg's continuous locomotion with wireless brain-to-brain interface. Sci Rep 9, 1321.

SUPPORTING INFORMATION

Figure S1 Animal pairs and flowchart of the signal transformation in the optical BtBI experiments.

Figure S2 Control experiments for optical BtBI.

Figure S3 The method of calculating information transfer rate.

Movie S1 An optical BtBI enables a Master mouse to control the locomotion of an Avatar mouse.

The supporting information is available online at http://life.scichina.com and https://link.springer.com. The supporting materials are published as submitted, without typesetting or editing. The responsibility for scientific accuracy and content remains entirely with the authors.